Robustness Assessment of Primal-dual Gradient Projection-based Online Feedback Optimization for Real-time Distribution Grid Management

Robustness Assessment of Primal-dual Gradient Projection-based Online Feedback Optimization for Real-time Distribution Grid Management

Sen Zhan[a,*], Johan Morren[a,b], Wouter van den Akker[a,c], Anne van der Molen[a,d], Nikolaos G. Paterakis[a], J. G. Slootweg[a,b]

[a]*Department of Electrical Engineering, Eindhoven University of Technology, Eindhoven, 5600 MB, The Netherlands*
[b]*Department of Asset Management, Enexis, 's-Hertogenbosch, 5223 MB, The Netherlands*
[c]*Corporate Strategy Department, Alliander, Arnhem, 6812 AH, The Netherlands*
[d]*Grid Strategy Department, Stedin, Rotterdam, 3011 TA, The Netherlands*

Abstract

The increasing deployment of distributed energy resources causes voltage and congestion issues in distribution grids. Recently, online feedback optimization (OFO) emerges as a promising real-time solution approach. OFO uses measurements as feedback and employs optimization algorithms as feedback controllers to steer the distribution system towards optimal operating points. OFO does not need an accurate grid model nor consumption data of non-controllable loads and affords fast implementation, which make it particularly suitable for real-time distribution grid management. This paper aims to provide an extensive robustness assessment of OFO based on the primal-dual gradient projection (PDGP) algorithm under practical distribution grid operational conditions. To quantify system performance, we use metrics including active power curtailment ratio, voltage and loading constraint violations, normalized reference power tracking error, and distance to the deterministic-case trajectory. Simulations conducted on a 136-bus medium-voltage grid using second-scale data reveal that the algorithm demonstrates satisfactory robustness to time-varying generation and loads, grid model inaccuracy, measurement errors, and communication failures, but is susceptible to systematic communication delays and unnoticed topology changes particularly involving tripping of cables at the beginning of distribution feeders. Potential solutions to these shortcomings are discussed.

Keywords: Online feedback optimization, autonomous optimization, congestion management, system balancing, robustness

1. Introduction

The proliferation of distributed energy resources (DERs) causes operational challenges for distribution system operators (DSOs), including network congestion and voltage limit violations. Today, the network capacity is becoming a bottleneck to the continuous deployment of DERs [1]. Grid reinforcement is the conventional solution approach. However, it requires significant investments, well-trained workforce and is a long-term process. An accompanying strategy is to actively exploit the flexibility from these DERs.

A classic modeling framework for this task is optimal power flow (OPF). Based on a distribution grid model, OPF can be used to derive the optimal active and reactive power setpoints of DERs given a predefined cost function. To represent and constrain voltages and loadings of cables and transformers within their limits, nonlinear, relaxed, or linearized power flow relations, which map DER setpoints and power consumption of non-controllable loads to voltages and loadings, are incorporated. While this framework, including its distributed implementations, has been well-studied [2], its applicability in the real-time distribution grid operational context is limited for several reasons. First, to construct an OPF model, an accurate grid topology is required, which is not always readily available to the DSO. Second, OPF takes real-time measurements of non-controllable loads as input, which can cause privacy concerns and these measurements are often not available either. Third, by the time the data collection and OPF computation are completed, the optimized setpoints might already have become outdated due to rapid variations of generation and loads. This becomes especially relevant when distributed optimization techniques are used which typically take tens to hundreds of communication rounds to reach convergence. Finally, a model-based feedforward approach generally lacks robustness to system uncertainties and disturbances [3, 4].

Online feedback optimization (OFO) overcomes these challenges, making it a promising real-time solution approach to distribution grid issues. Unlike the traditional offline approach of waiting for the algorithm to converge, OFO enables rapid deployment of new setpoints to inverter-interfaced DERs. This is facilitated by integrating voltage and power flow measurements into a closed-loop feedback system; see Fig. 1 for a schematic overview of a feedback system and comparison to a model-based feedforward system. Compared to local droop control approaches, OFO ensures grid constraint satisfaction [5]. Compared to deep reinforcement learning approaches [6–9], OFO does not need a complicated (often offline centralized)

*Corresponding author
Email addresses: s.zhan@tue.nl (Sen Zhan), j.morren@tue.nl (Johan Morren), w.f.v.d.akker@tue.nl (Wouter van den Akker), a.e.v.d.molen@tue.nl (Anne van der Molen), n.paterakis@tue.nl (Nikolaos G. Paterakis), j.g.slootweg@tue.nl (J. G. Slootweg)

training process and has guarantees to pursue globally optimal solutions [10–13].

Existing OFO controllers are designed utilizing algorithms such as gradient projection with soft penalty functions [14–20], gradient projection with barrier functions [21], gradient projection [22–26], dual ascent [5, 27–33], primal-dual gradient projection [10–12, 34–42], and Newton-based second-order methods [43, 44]; see also our recent survey paper [45]. The various OFO algorithms, mostly, differ in the way they handle output constraints such as voltage and loading limits. With soft penalty or barrier functions, constraint violations are penalized in the objective function. While using soft penalty functions can result in prolonged constraint violations, using barrier functions requires an additional iterative process over the barrier parameter and may not be suitable for the online implementation under time-varying grid conditions. In gradient projection, gradient iterates are projected onto a linearized feasible region around the current operating point. While this approach requires less parameter tuning and shows benign convergence behavior [3], it leads to centralized calculations. In primal-dual methods, output constraints are dualized, affording a distributed implementation [4]. This feature renders them particularly suitable for real-time distribution grid management. Compared to dual ascent, the primal-dual gradient projection (PDGP) algorithm offers the flexibility to tune the step size for the primal variable update step.

Various sources of uncertainties such as grid model inaccuracy, measurement errors, communication failures and delays, topology changes, and time-varying generation and loads may jeopardize the performance of OFO. Therefore, it is imperative to assess the robustness of OFO to those uncertainties which may be present in practical distribution grid operational conditions. For grid model inaccuracy, a theoretic robustness analysis is provided in [20], which is based on OFO with a soft penalty function. Numerical and experimental evidence showing the robustness of OFO has also been presented in the literature, which we summarize in Table 1. To improve the algorithm performance under measurement errors and model uncertainty, state estimation and online sensitivity estimation methods have been advocated in [16–19]. Furthermore, the studies in [36, 39, 46] eliminated the need of grid models leveraging zeroth-order optimization techniques which derive unbiased estimates of gradients only using evaluations of the function. Finally, in case of communication failures, a *freezing* strategy has been reported in [12, 41, 47] which implies using the latest information.

Outlined in Table 1, our study aims to provide more extensive simulations to evaluate the robustness of OFO against various uncertainties. These simulations confirm some existing results, challenge some other, and provide new findings. We leverage the PDGP algorithm which features a gather-and-broadcast communication architecture and distributed calculations and is considered well-suited for distribution grids due to reduced privacy concerns. Our investigation centers on two applications of OFO: congestion management which aims to enforce voltage and current limits in distribution grids, and balancing service provision in the form of tracking given active power setpoints from transmission system operators (TSOs).

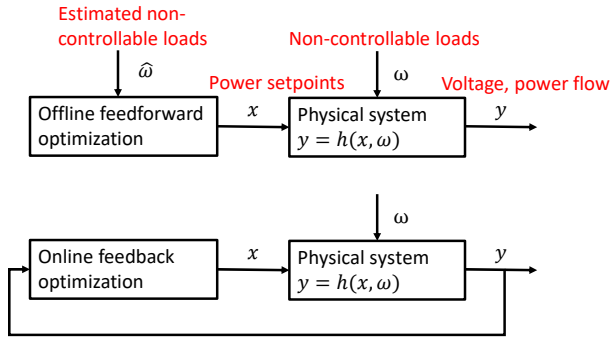

Figure 1: Block diagrams of an open-loop feedforward and a closed-loop feedback system, where x represents system input, y represents system output, ω ($\widehat{\omega}$) represents (estimated) system disturbance, and h maps system input and disturbance to system output. Figure is adapted from [22].

We quantify system performance using metrics including active power curtailment, constraint violations, tracking error, and deviation from the deterministic case. As [2] points out, such numerical simulations are pivotal for gaining insights into the practical performance of various algorithms. In a broader context, similar numerical studies have been conducted to assess the impact of non-ideal communication on distributed optimization algorithms including augmented Lagrangian-based algorithms [48] and the equivalent network approximation method [49].

To summarize, the main contributions of this paper are:

- Extensive simulations are conducted to evaluate the robustness of OFO under various sources of uncertainty in practical distribution systems. The OFO implementation based on the PDGP algorithm enables fast, distributed calculations and requires only basic arithmetic operations. The investigated uncertainty sources include time-varying generation and loads, grid model inaccuracy, measurement errors, communication failures and delays, and unnoticed topology changes.

- Quantification metrics are developed to assess the impact on power curtailment, distribution system constraint violations, reference power tracking error, and deviation from the deterministic case.

- Potential solutions to the identified shortcomings of OFO are discussed.

The remainder of this paper is structured as follows: Section 2 presents the optimization problem and the feedback-based primal-dual gradient projection algorithm. Section 3 provides system performance quantification metrics. Section 4 describes the case study and modeling of system uncertainties. Section 5 presents simulation results. Finally, Section 6 concludes this study.

2. Methodology

This section starts with introducing notations, followed by a real-time optimization problem where the power flow relations

Table 1: Overview of numerical and experimental studies of OFO. MD: inaccurate grid models; MS: measurement errors; CF: communication failures; CD: communication delays; TP: unobserved topology changes; TV: time-varying generation and loads.

Ref	Variables	Methodology	Grid limits	Balancing	Uncertainties
Zhu 2016 [14]	Q	Soft penalty	Voltage	✗	TV
Hauswirth 2017 [15]	P, Q	Soft penalty	Voltage, current	✗	TV
Picallo 2020 [16]	P, Q	Soft penalty	Voltage	✗	MS, TV
Picallo 2022 [17]	P, Q	Soft penalty	Voltage	✗	MD, TV
Cheng 2022 [18]	Q	Soft penalty	Voltage	✗	MD, TV
Xu 2023 [19]	Q	Soft penalty	Voltage	✗	MD, MS, TV
Colombino 2019 [20]	P, Q	Soft penalty	Voltage	✗	MD, TV
Gan 2016 [21]	P, Q	Barrier function	Voltage	✗	✗
Ortmann 2023 [22]	P, Q	Gradient projection	Voltage, current	✗	MD, TV
Ortmann 2023 [23]	P, V	Gradient projection	Voltage, current	✗	TP, TV
Klein-Helmkamp 2023 [24]	P, Q	Gradient projection	Voltage	✓	TV
Ortmann 2024 [25]	P, Q	Gradient projection	Voltage	✓	TV
Cave 2024 [26]	P,Q	Gradient projection	Voltage, current	✗	MD, MS, CD, TV
Bolognani 2015 [27]	Q	Dual ascent	Voltage	✗	TV
Bolognani 2019 [5]	Q	Dual ascent	Voltage	✗	TV
Ortmann 2020 [28]	Q	Dual ascent	Voltage	✗	TV
Ortmann 2020 [29]	Q	Dual ascent	Voltage	✗	MD, TV
Zhou 2020 [30]	P, Q	Dual ascent	Voltage	✗	TV
Tang 2021 [31]	Q	Dual ascent	Voltage	✗	TV
Magnusson 2020 [32]	P, Q	Dual ascent	Voltage	✗	MD, MS, CF, CD, TV
Patari 2022 [33]	P, Q	Dual ascent	Voltage	✗	MD, MS, CF, CD, TV
Dall'Anese 2018 [10]	P, Q	Primal-dual	Voltage	✗	TV
Dall'Anese 2018 [11]	P, Q	Primal-dual	Voltage	✓	TV
Zhou 2018 [34]	P, Q	Primal-dual	Voltage	✗	TV
Bernstein 2019 [12]	P, Q	Primal-dual	Voltage, current	✓	CD, TV
Qu 2020 [35]	Q	Primal-dual	Voltage	✗	MD, MS, CD, TV
Chen 2020 [36]	P, Q	Primal-dual	Voltage	✓	MD, MS, TV
Ipach 2022 [37]	P, Q	Primal-dual	Voltage, current	✗	CF, CD, TV
Zhao 2022 [38]	P, Q	Primal-dual	Voltage	✗	TV
Hu 2023 [39]	Q	Primal-dual	Voltage	✗	MD, CD, TV
Zhan 2023 [40]	P, Q	Primal-dual	Voltage, current	✗	MD, CF, TV
Panahazari 2023 [41]	P, Q	Primal-dual	Voltage	✓	CF, CD, TV
Guo 2023 [13]	P,Q	Primal-dual	Voltage	✗	MS
Zhan 2024 [42]	P, Q	Primal-dual	Voltage, current	✗	TV
Tang 2017 [43]	P, Q	Soft penalty (Newton)	Voltage, current	✗	TV
Cheng 2022 [44]	Q	Soft penalty (Newton)	Voltage	✗	TV
This paper	P, Q	Primal-dual	Voltage, current	✓	MD, MS, CF, CD, TP, TV

are implicitly represented, and the PDGP algorithm to solve the problem with a feedback-based implementation.

2.1. Notation

Consider a distribution grid with $N+1$ buses collected in the set $\mathcal{N} := \{0, 1, \cdots, N\}$, and cables represented by the set $\mathcal{E} := \{(i, j)\} \subset \mathcal{N} \times \mathcal{N}$. Define $\mathcal{N}^+ := \mathcal{N} \backslash \{0\}$, where bus 0 is the substation bus and is assumed to have a fixed voltage. Denote by $\mathcal{N}_G \subseteq \mathcal{N}^+$ the set of buses where renewable generation units such as photovoltaics and small-scale wind turbines are located, and by $\mathcal{N}_M \subseteq \mathcal{N}^+$ and $\mathcal{E}_M \subseteq \mathcal{E}$ the sets of monitored buses and cables (with voltage and power flow measurements available), respectively. For each bus $i \in \mathcal{N}_G$, denote by p_i and q_i the active and reactive power generation, and by $\overline{P}_j$ and $\overline{S}_j$ the maximum active power generation and inverter capacity, respectively. For each bus $i \in \mathcal{N}^+$, denote by p_i^d and q_i^d the active and reactive power demand. Let v_j be the magnitude of the complex voltage phasor for each bus $j \in \mathcal{N}_M$, and let $\underline{v}$ and $\overline{v}$ be its lower and upper limits, respectively. For each cable $(i, j) \in \mathcal{E}_M$, denote by P_{ij} and Q_{ij} the active and reactive power flow from bus i to j, respectively, and by $\overline{S}_{ij}$ its capacity. For the transformer, denote by P_{trafo} and Q_{trafo} the active and reactive power flow, respectively, and by $\overline{S}_{trafo}$ its capacity. Finally, upper-case (lower-case) boldface letters will be used for matrices (column vectors) with appropriate components defined earlier, e.g. $\mathbf{v} := [v_i, i \in \mathcal{N}_M]^\intercal$, and $\mathbf{p} := [p_i, i \in \mathcal{N}_G]^\intercal$.

2.2. Optimization model

A real-time optimization problem, which aims to derive the optimal active and reactive power setpoints of renewable generation units while adhering to distribution grid limits and following some reference active power setpoint from the TSO if

requested, is formulated in (1). Specifically, the objective function f in (1a) concerns active power curtailment and reactive power use, where ξ is a sufficiently small positive weighting factor that prioritizes reactive power use over active power curtailment. Constraints (1b)-(1d) ensure that voltages, cable loadings, and the transformer loading remain within their limits, respectively. Note that the power flow terms, e.g. P_{ij} and Q_{ij}, which denote the active and reactive power flow from bus i to j respectively, can be both positive and negative, reflecting bi-directional power flow due to distributed generation. These constraints are essential to prevent voltage limit violations, congestion and maintain network security, which is especially important in modern distribution grids with growing DER connections. If requested, (1e) guarantees adherence to the reference active power setpoint through the transformer dictated by the TSO. In (1b)-(1e), μ_i, λ_i, ρ_{ij}, ρ_{trafo}, and π represent the respective dual variables (also known as the Lagrangian multipliers) associated with the constraints, which indicate how much the objective function would drop if the constraints were slightly relaxed, i.e. they capture the sensitivity of their respective constraints. Note that the system state variables including voltages and active and reactive power flow are dependent, through some implicit function, on the active and reactive power setpoints of renewable generation units and power consumption of non-controllable loads. Finally, (1f) ensures satisfaction of the operational limit of renewable generation units.

$$\underset{p_i,q_i,\forall i\in\mathcal{N}_G}{\text{minimize}} f := \frac{1}{2}\sum_{i\in\mathcal{N}_G}(\overline{P}_i - p_i)^2 + \frac{1}{2}\xi\sum_{i\in\mathcal{N}_G} q_i^2, \tag{1a}$$

$$s.t.\ \underline{v} \le v_i \le \overline{v} : \mu_i, \lambda_i, \forall i \in \mathcal{N}_M, \tag{1b}$$

$$\ell_{ij} := \sqrt{P_{ij}^2 + Q_{ij}^2} \le \overline{S}_{ij} : \rho_{ij}, \forall (i,j) \in \mathcal{E}_M, \tag{1c}$$

$$\ell_{trafo} := \sqrt{P_{trafo}^2 + Q_{trafo}^2} \le \overline{S}_{trafo} : \rho_{trafo}, \tag{1d}$$

$$P_{trafo} = \dot{P}_{trafo} : \pi, \tag{1e}$$

$$(p_i, q_i) \in \mathcal{X}_i, \forall i \in \mathcal{N}_G, \text{ where} \tag{1f}$$

$$\mathcal{X}_i := \{(p,q) : 0 \le p \le \overline{P}_i, p^2 + q^2 \le \overline{S}_i^2\}.$$

Remark 1. In Problem (1) and following simulations, we focus on utilizing renewable generation units to address voltage and congestion issues which are often also caused by them and provide grid services to TSOs. Notably, many regions in the Netherlands are experiencing insufficient grid capacity to accommodate increasing renewable generation [50]. The amount of active power curtailment further serves as a direct metric to evaluate the impact of control and various uncertainties on end-users. Nevertheless, OFO is readily applicable to control load units such as electric vehicles and battery energy storage [11, 12, 36, 42].

2.3. Online feedback optimization

Unlike model-based approaches where a power flow model is supplied to Problem (1), OFO uses measurements as feedback and leverages optimization algorithms as feedback controllers [4] to drive the physical distribution system towards the optimal operating point defined by Problem (1). In this paper, we implement OFO utilizing the PDGP algorithm which features distributed calculations and a gather-and-broadcast communication architecture [36]. Before presenting the algorithm, the dual problem of (1) is given in (2):

$$\underset{\boldsymbol{\lambda}\ge\mathbf{0},\boldsymbol{\mu}\ge\mathbf{0},\boldsymbol{\rho}\ge\mathbf{0},\rho_{trafo}\ge 0,\pi\in\mathbb{R}}{\text{maximize}} \Big\{ \underset{(p_i,q_i)\in\mathcal{X}_i,i\in\mathcal{N}_G}{\text{minimize}} \mathcal{L}(\mathbf{p},\mathbf{q},\boldsymbol{\lambda},\boldsymbol{\mu},\boldsymbol{\rho},\rho_{trafo},\pi) \Big\}, \tag{2}$$

where the partial Lagrangian function $\mathcal{L}$ is given in (3):

$$\begin{aligned}\mathcal{L}(\mathbf{p},\mathbf{q},\boldsymbol{\lambda},\boldsymbol{\mu},\boldsymbol{\rho},\rho_{trafo},\pi) &:= f + \sum_{i\in\mathcal{N}_M}\lambda_i(v_i - \overline{v}) \\ &+ \sum_{i\in\mathcal{N}_M}\mu_i(\underline{v} - v_i) + \sum_{(i,j)\in\mathcal{E}_M}\rho_{ij}\left(\sqrt{P_{ij}^2 + Q_{ij}^2} - \overline{S}_{ij}\right) \\ &+ \rho_{trafo}\left(\sqrt{P_{trafo}^2 + Q_{trafo}^2} - \overline{S}_{trafo}\right) \\ &+ \pi(P_{trafo} - \dot{P}_{trafo}).\end{aligned} \tag{3}$$

While several papers [10–12, 36] leveraged regularized Lagrangian functions to establish theoretical convergence results, we find in our simulations that the impact of some small regularization factors (e.g. $\sim 10^{-4}/10^{-3}$) on our numerical results is negligible and the algorithm works well without regularization.

At its core, the PDGP algorithm performs projected gradient ascent and descent for the dual and primal variables, respectively. At each time step (iteration) k, it includes the following five steps:

1. For each bus $i \in \mathcal{N}_M$, collect its voltage measurement $\tilde{v}_i^k$ and update λ_i and μ_i, where the projection operator is defined as $[u]^+ := \max(u, 0)$ and α with various superscripts represents step sizes:

$$\lambda_i^{k+1} \leftarrow [\lambda_i^k + \alpha^\lambda(\tilde{v}_i^k - \overline{v})]^+, \tag{4a}$$

$$\mu_i^{k+1} \leftarrow [\mu_i^k + \alpha^\mu(\underline{v} - \tilde{v}_i^k)]^+. \tag{4b}$$

2. For each cable $(i,j) \in \mathcal{E}_M$, collect its active and reactive power measurements $\tilde{P}_{ij}^k$ and $\tilde{Q}_{ij}^k$ and update ρ_{ij}, where $\tilde{S}_{ij}^k = \sqrt{(\tilde{P}_{ij}^k)^2 + (\tilde{Q}_{ij}^k)^2}$:

$$\rho_{ij}^{k+1} \leftarrow [\rho_{ij}^k + \alpha^\rho(\tilde{S}_{ij}^k - \overline{S}_{ij})]^+. \tag{4c}$$

3. For the substation transformer, collect its active and reactive power measurements $\tilde{P}_{trafo}^k$ and $\tilde{Q}_{trafo}^k$ and update ρ_{trafo}, where $\tilde{S}_{trafo}^k = \sqrt{(\tilde{P}_{trafo}^k)^2 + (\tilde{Q}_{trafo}^k)^2}$:

$$\rho_{trafo}^{k+1} \leftarrow [\rho_{trafo}^k + \alpha^{\rho_{trafo}}(\tilde{S}_{trafo}^k - \overline{S}_{trafo})]^+; \tag{4d}$$

if balancing service is requested by the TSO, update π:

$$\pi^{k+1} \leftarrow \pi^k + \alpha^\pi(\tilde{P}_{trafo}^k - \dot{P}_{trafo}). \tag{4e}$$

4. The DSO broadcasts the updated dual variables λ_i^{k+1}, μ_i^{k+1}, ρ_{ij}^{k+1}, ρ_{trafo}^{k+1}, and π^{k+1} and power flow measurements $\tilde{P}_{ij}^k$, $\tilde{Q}_{ij}^k$, $\tilde{P}_{trafo}^k$, and $\tilde{Q}_{trafo}^k$.

5. For each generator $i \in \mathcal{N}_G$, update its active and reactive power setpoints p_i and q_i, where the projection operator parameterized by a positive definite matrix $\mathbf{G}$ [51] is defined as $\text{proj}^{\mathbf{G}}_{\mathcal{X}}[\mathbf{u}] := \underset{\mathbf{x}\in\mathcal{X}}{\text{argmin}}(\mathbf{x}-\mathbf{u})^\intercal\mathbf{G}(\mathbf{x}-\mathbf{u})$:

$$\begin{bmatrix} p_i^{k+1} \\ q_i^{k+1} \end{bmatrix} \leftarrow \text{proj}^{\mathbf{G}}_{\mathcal{X}_i^k}\left\{\begin{bmatrix} p_i^k \\ q_i^k \end{bmatrix} - \alpha\mathbf{G}^{-1}\nabla_{[p_i,q_i]}\mathcal{L}^k\Big|_{p_i^k,q_i^k,\lambda^{k+1},\boldsymbol{\mu}^{k+1},\boldsymbol{\rho}^{k+1},\rho_{trafo}^{k+1},\pi^{k+1}}\right\}. \tag{4f}$$

Components of the above gradient are specified in (5) as:

$$\begin{aligned}\frac{\partial\mathcal{L}^k}{\partial p_i} &= p_i^k - \overline{P}_i + \sum_{i\in\mathcal{N}_M}(\lambda_i^{k+1}-\mu_i^{k+1})\frac{\partial v_i}{\partial p_i} \\ &+ \sum_{(m,n)\in\mathcal{E}_M}\rho_{mn}^{k+1}\frac{\tilde{P}_{mn}^k}{\tilde{S}_{mn}^k}\frac{\partial P_{mn}}{\partial p_i} + \sum_{(m,n)\in\mathcal{E}_M}\rho_{mn}^{k+1}\frac{\tilde{Q}_{mn}^k}{\tilde{S}_{mn}^k}\frac{\partial Q_{mn}}{\partial p_i} \\ &+ \rho_{trafo}^{k+1}\frac{\tilde{P}_{trafo}^k}{\tilde{S}_{trafo}^k}\frac{\partial P_{trafo}}{\partial p_i} + \rho_{trafo}^{k+1}\frac{\tilde{Q}_{trafo}^k}{\tilde{S}_{trafo}^k}\frac{\partial Q_{trafo}}{\partial p_i} \\ &+ \pi^{k+1}\frac{\partial P_{trafo}}{\partial p_i},\end{aligned} \tag{5a}$$

$$\begin{aligned}\frac{\partial\mathcal{L}^k}{\partial q_i} &= \xi q_i^k + \sum_{i\in\mathcal{N}_M}(\lambda_i^{k+1}-\mu_i^{k+1})\frac{\partial v_i}{\partial q_i} \\ &+ \sum_{(m,n)\in\mathcal{E}_M}\rho_{mn}^{k+1}\frac{\tilde{P}_{mn}^k}{\tilde{S}_{mn}^k}\frac{\partial P_{mn}}{\partial q_i} + \sum_{(m,n)\in\mathcal{E}_M}\rho_{mn}^{k+1}\frac{\tilde{Q}_{mn}^k}{\tilde{S}_{mn}^k}\frac{\partial Q_{mn}}{\partial q_i} \\ &+ \rho_{trafo}^{k+1}\frac{\tilde{P}_{trafo}^k}{\tilde{S}_{trafo}^k}\frac{\partial P_{trafo}}{\partial q_i} + \rho_{trafo}^{k+1}\frac{\tilde{Q}_{trafo}^k}{\tilde{S}_{trafo}^k}\frac{\partial Q_{trafo}}{\partial q_i} \\ &+ \pi^{k+1}\frac{\partial P_{trafo}}{\partial q_i}.\end{aligned} \tag{5b}$$

Remark 2. The PDGP algorithm has very light computation power and memory requirements. Steps 1-3 are performed in parallel and involve only basic arithmetic operations. Step 5 is also conducted in parallel at each controllable generation unit. Its projection operation is realized by solving a two-variable convex quadratic program, for which our earlier work [40] provides an efficient iterative algorithm.

Remark 3. The PDGP-based controller requires tuning of various step sizes $\{\alpha, \alpha^\lambda, \alpha^\mu, \alpha^\rho, \alpha^{\rho_{trafo}}, \alpha^\pi\}$ and the positive definite matrix $\mathbf{G}$ to accelerate its convergence and improve its dynamic performance; refer to [25] for a detailed discussion on tuning $\mathbf{G}$. While too small step sizes result in slow convergence, too large step sizes lead to instability. The guideline for the choice of the matrix $\mathbf{G}$ is that it should approximate the Hessian of the Lagrangian function $\mathcal{L}$ over p_i and q_i [51]. For simplicity, a diagonal matrix is usually chosen. We find in our simulations that the algorithm works well with a large range of step sizes and choices of $\mathbf{G}$. We conjecture that this is due to its feedback-based nature.

3. Performance Evaluation Metrics

To assess the impact of uncertainties, the following metrics are developed to quantify system performance. Specifically, we use the active power curtailment, constraint violations, and tracking error to quantify the impact on the end-users, DSO, and TSO, respectively.

Active power curtailment

This reflects interest of end-users. The active power curtailment ratio (APCR) is defined in (6a) as the ratio between the total power curtailment and maximum power generation. Its value lies in the interval [0, 1].

$$\text{APCR} = \frac{\sum_{k\in\mathcal{K}}\sum_{i\in\mathcal{N}_G}(\overline{P}_i^k - p_i^k)}{\sum_{k\in\mathcal{K}}\sum_{i\in\mathcal{N}_G}\overline{P}_i^k}. \tag{6a}$$

Constraint violations

Satisfaction of voltage, cable loading, and transformer loading limits represents a requirement of the DSO. Definitions of the average voltage violation (AVV), average loading violation of cables (ALVC), and average loading violation of the transformer (ALVC) are given in (6b)-(6d), respectively. The projection operator ensures that only constraint violations are accumulated.

$$\text{AVV} = \frac{1}{|\mathcal{K}||\mathcal{N}_M|}\sum_{k\in\mathcal{K}}\sum_{i\in\mathcal{N}_M}\left([v_i^k - \overline{v}]^+ + [\underline{v} - v_i^k]^+\right). \tag{6b}$$

$$\text{ALVC} = \frac{1}{|\mathcal{K}||\mathcal{E}_M|}\sum_{k\in\mathcal{K}}\sum_{(i,j)\in\mathcal{E}_M}\left([\ell_{ij}^k - \overline{\ell}]^+\right). \tag{6c}$$

$$\text{ALVT} = \frac{1}{|\mathcal{K}|}\sum_{k\in\mathcal{K}}\left([\ell_{trafo}^k - \overline{\ell}_{trafo}]^+\right). \tag{6d}$$

Reference tracking error

Tracking of the reference active power setpoint $\dot{P}_{trafo}^k$ is considered important to the TSO, if requested. For this, the normalized root mean squared error (NRMSE) is defined in (6e).

$$\text{NRMSE} = \sqrt{\frac{1}{|\mathcal{K}|}\sum_{k\in\mathcal{K}}\left(\frac{P_{trafo}^k - \dot{P}_{trafo}^k}{\dot{P}_{trafo}^k}\right)^2}. \tag{6e}$$

Distance to the deterministic-case trajectory

Finally, the distance to the deterministic-case trajectory $(p_i^{k^*}, q_i^{k^*})$ where no uncertainties are present is defined in (6f) using the root mean squared deviation (RMSD).

$$\text{RMSD} = \sqrt{\frac{1}{2|\mathcal{K}||\mathcal{N}_G|}\sum_{k\in\mathcal{K}}\sum_{i\in\mathcal{N}_G}\left[(p_i^k - p_i^{k^*})^2 + (q_i^k - q_i^{k^*})^2\right]}. \tag{6f}$$

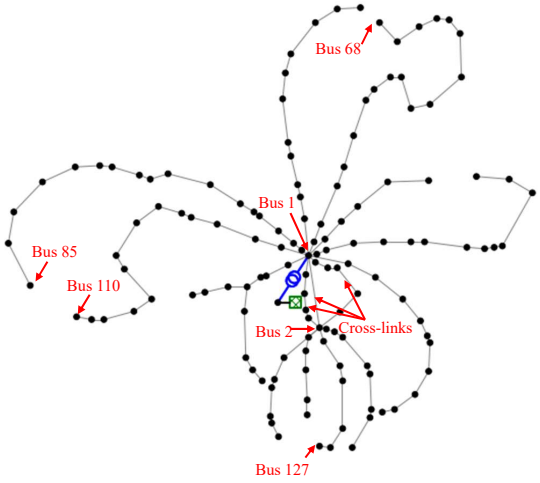

Figure 2: A 136-bus medium-voltage grid from Simbench [52]. The green square marks the substation bus. Locations of the substation bus and a few other buses are modified for clarity.

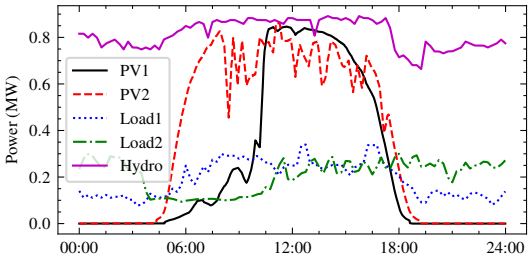

Figure 3: Hydropower and two example PV and load profiles. For visualization, hydropower output is reduced by 2 MW.

4. Case Description

The objective of this case study is to evaluate the robustness of OFO under various uncertainties in distribution grids. Particularly, OFO is used to derive active and reactive power setpoints of renewable generation units such that their active power curtailment is minimized while network and tracking constraints are satisfied.

4.1. Test data

Simulations are performed on a synthetic urban 136-bus medium-voltage (10-kV) grid from Simbench [52], shown in Fig. 2. The test grid has an open ring topology and cross-links between buses 1 and 2. Two 63-MVA HV/MV transformers are installed. The cable impedance and capacity data are the same as those in the original dataset. Following the dataset, the test grid is assumed to be balanced; however, the algorithm also works for unbalanced grids since no explicit power flow relations are required in (1). The capacities of 133 distributed renewable generation units, in this case photovoltaics (PVs), are scaled by a factor of 5, reaching 121 MW in total. A 2.9-MW hydropower plant is also connected, which is not controlled in the considered timescale. The total nominal load is 69 MW. Time series PV generation data are generated using the HelioClim3 dataset [53] with a 1-minute resolution for a sunny

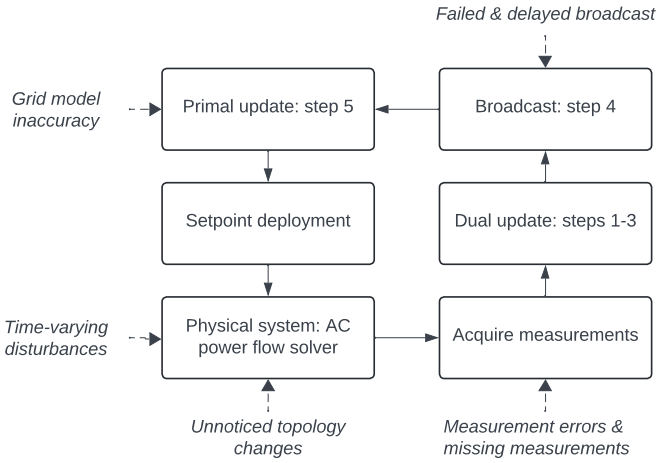

Figure 4: Sources of uncertainties in an OFO iteration.

day. Hydropower generation and load data from Simbench with a 15-minute resolution are linearly interpolated into profiles with a 1-minute resolution. In Fig. 3, hydropower and example PV and load profiles are visualized, showing their variability.

The lower and upper voltage limits $\underline{v}$ and $\overline{v}$ are set as 0.95 and 1.05 pu, respectively. The loading limit for cables is 100%, while that for each of the two HV/MV transformers is 50% according to the original dataset. The reactive power weighting factor ξ is set to 0.1. The step sizes and the scaling matrix $\mathbf{G}$ are chosen as $\alpha = 0.1$, $\alpha^{\lambda} = \alpha^{\mu} = 100$, $\alpha^{\rho} = \alpha^{\rho_{trafo}} = \alpha^{\pi} = 10$, and $\mathbf{G} = \begin{bmatrix} 1 & 0 \\ 0 & 0.2 \end{bmatrix}$ using a trial-and-error strategy [35]. An OFO iteration is executed every 6 seconds, yielding updated active and reactive PV power setpoints.

All simulations are performed on a standard PC with an Intel i7-9750H processor and a 16-GB RAM. Power flow calculations are implemented with the high-performance Python library Power-Grid-Model [54, 55]. A series implementation of the time series simulation for a day including in total 14400 iterations takes 30 seconds, averaging 2 milliseconds per iteration. This demonstrates the high computational efficiency of the algorithm and its suitability for real-time control.

4.2. Sensitivity matrices

Define $\mathbf{h}_P := [P_{ij}, (i,j) \in \mathcal{E}_M, P_{trafo}]^\intercal$ and $\mathbf{h}_Q := [Q_{ij}, (i,j) \in \mathcal{E}_M, Q_{trafo}]^\intercal$. By the definition of the Lagrangian function (3), computing (4f) requires evaluating $\nabla_{\mathbf{p}}\mathbf{v}$, $\nabla_{\mathbf{q}}\mathbf{v}$, $\nabla_{\mathbf{p}}\mathbf{h}_P$, $\nabla_{\mathbf{q}}\mathbf{h}_P$, $\nabla_{\mathbf{p}}\mathbf{h}_Q$, and $\nabla_{\mathbf{q}}\mathbf{h}_Q$, which are the power-to-voltage and power-to-branch flow sensitivity matrices. These matrices evolve over time with varying generation and loads. In OFO, one can usually approximate them with constant matrices due to its feedback-based virtue, which brings robustness to model mismatch [20, 29]. In this study, we build these approximations by running a series of perturbations around an operating point using a distribution grid model and power flow calculations. This allows OFO to work with any test system regardless of its topology.

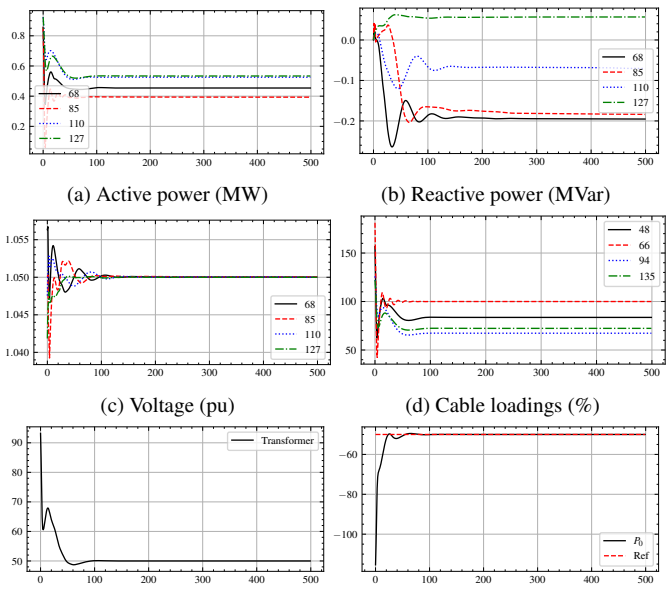

(a) Active power (MW) (b) Reactive power (MVar)

(c) Voltage (pu) (d) Cable loadings (%)

(e) Transformer loading (%) (f) HV/MV transformer (MW)

Figure 5: Convergence of the algorithm under static loading for 500 iterations. Results are shown for 4 buses located towards the feeder ending and 4 cables located at the beginning. Numbered legends represent indices of buses/cables.

4.3. Uncertainty modeling

The following sources of uncertainties in practical distribution grids are considered in this study, which are summarized in Fig. 4 for an OFO iteration.

Time-varying generation and loads

Generation and loads in distribution grids are particularly volatile. OFO often does not converge before generation and load profiles have changed. In this study, at most 10 OFO iterations are run for each generation and load data point in the time series profile. This simulates the performance of OFO at a time-varying environment.

Grid model inaccuracy

Two modeling methods are applied to simulate the grid model inaccuracy. The first method assumes that the modeling errors are normally distributed. Therefore, Gaussian noise with a standard deviation of σ_s is added to the sensitivity matrices. The second method assumes that the errors conform to a uniform distribution as in [32, 33, 35]. For example, the voltage sensitivity $\frac{\partial v_i}{\partial p_j}$ is modeled using (7).

$$\frac{\partial v_i}{\partial p_j} \leftarrow \frac{\partial v_i}{\partial p_j}(1+\omega_{ij}), \text{where } \omega_{ij} \sim \mathcal{N}\left(0, \sigma_s^2\right) \text{ or } \omega_{ij} \sim \mathcal{U}\left(-\sigma_s, \sigma_s\right). \tag{7}$$

Measurement errors

As in [19, 32, 33, 35], Gaussian white noise with a standard deviation of σ_m is added to the measured voltages and power flow.

Communication failures

These include missing measurements and failed broadcast steps. A probability of failing *pr* is assigned to each measurement and each broadcast step. In case of a missing measurement, the corresponding dual variable is not updated. In case of failed broadcast, the latest available dual information is used for primal update.

Communication delays

For this, we assume the broadcasted information is delayed for τ steps. That is, at time step k, dual information from time step $k-\tau$ is actually used.

Topology changes

We investigate cases where a cable trips and a normally-open switch is closed while restoring all loads. In total, 307 possible cases are examined for the test grid. Note that the sensitivity matrices are kept unchanged to simulate a scenario where such a network reconfiguration is not known by the DSO.

5. Results

5.1. Static case

In the static case, no uncertainties are present to the controller to study its convergence. Figure 5 demonstrates quick system constraint satisfaction and convergence of the algorithm after approximately 250 iterations. Active and reactive power, voltages, and cable and transformer loadings are shown in Figs. 5a-5e without reference power tracking. The upper voltage limit of 1.05 pu, the cable loading limit of 100%, and the transformer loading limit of 50% are successfully enforced. Active power generation from PVs is curtailed, while reactive power is either injected to reduce reactive power transfer to reduce cable and transformer loadings or absorbed to lower voltage magnitudes. The diverse behavior observed in reactive power is captured by Problem (1) and depends on the feeder characteristics. For longer feeders, voltage constraints tend to be active, while for shorter but denser feeders, loading constraints tend to be active. Figure 5f shows reference power tracking at the HV/MV transformer when a reference setpoint of -50 MW is asked by the TSO.

5.2. Time-varying deterministic case

In the context of OFO, one does not wait for the algorithm to converge. Instead, the system output is continuously measured and the system input is immediately adjusted. In our simulation, the time series generation and load data have a resolution of one minute. Per 6 seconds, an OFO iteration is run, indicating that 10 OFO iterations are implemented per generation and load data point. This is often not sufficient for the algorithm to converge. Figure 6 shows the performance of OFO in such a time-varying simulation. Figure 6a shows the active power curtailment where more curtailment occurs around 12:00 because of the tighter export limit from reference power tracking as shown in Fig. 6f. Figure 6b shows the diverse behavior in reactive power as explained above without reference tracking.

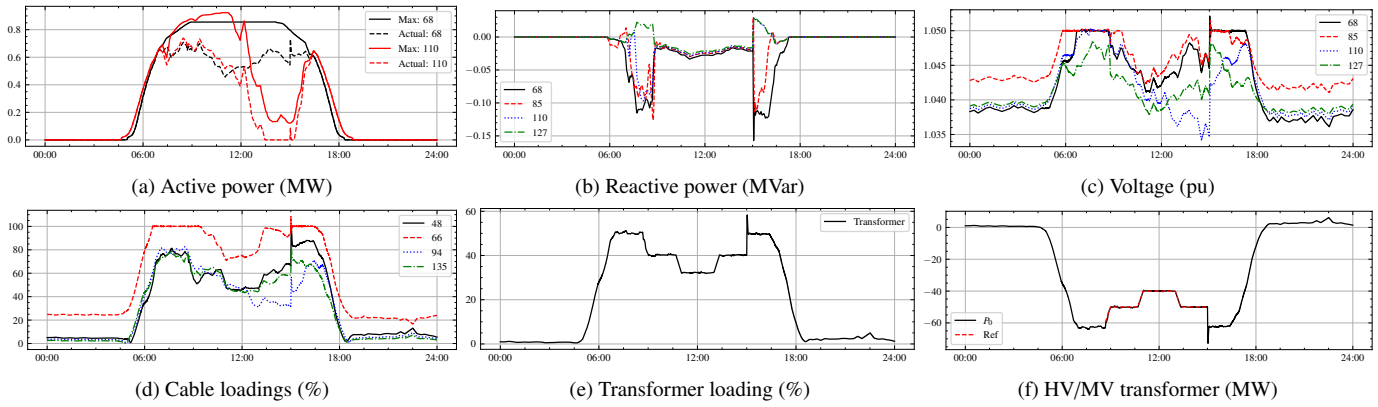

(a) Active power (MW) (b) Reactive power (MVar) (c) Voltage (pu)

(d) Cable loadings (%) (e) Transformer loading (%) (f) HV/MV transformer (MW)

Figure 6: Trajectories of the algorithm under time-varying grid loading for a day. One OFO iteration is executed every 6 seconds. Numbered legends represent indices of buses/cables.

When reference tracking is required, all units consume reactive power to increase network losses to limit export. Figures 6c-6e show grid constraint satisfaction (AVV and ALVC are both negligible, ALVT = 0.07%). Figure 6f shows that the time-varying reference power setpoints from 8:40 to 15:00 are tracked well (NRMSE = 0.70%). Noticeably an overshoot occurs when the tracking signal ends, which is quickly suppressed.

Figure 7 shows the various metrics under different uncertainties under the time-varying simulation, where Fig. 7a shows that the controller performance deteriorates with slower OFO update rates resulting in higher constraint violations and reference tracking error, which is consistent with the results in [40, 41]. The optimal update rate depends on dynamics of distribution grids, communication infrastructure, and actuation speed of inverters, and may require a cost-effectiveness analysis.

5.3. Grid model inaccuracy

Figures 7b and 7c show that the varying Gaussian and uniform noise added to the sensitivity matrices does not noticeably impact system performance. RMSD values suggest that PV inverters are actuated increasingly differently than in the deterministic case. This, however, does not result in higher power curtailment, constraint violations, or reference tracking error. Such robustness to model inaccuracy, as also demonstrated in for example [29, 35], is credited to its feedback-based implementation, and is not expected in model-based approaches.

5.4. Measurement errors

Using reference power tracking as an example, Fig. 8 illustrates how measurement errors propagate through the system and affect system output without inducing instability. Figure 7d further shows that the constraint violations and tracking error increase mildly with measurement errors. With 1% (standard deviation) measurement noise, the system performance is only slightly affected. This demonstrates robustness of the algorithm against random measurement errors. This aligns with the results in [26, 35]. To eliminate the potential impact of measurement errors, one can also connect a state estimator with OFO as suggested in [13, 16].

5.5. Communication failures

We consider missing measurements and failures in the broadcast step. When a measurement is missing, the corresponding dual variable stays the same. When the broadcast step fails, the latest available information is used to update PV setpoints. These introduce random delays of the dual variables. Our strategy represents an asynchronous algorithm and is similar to the cyber-resilient algorithm in [41]. Figures 7e and 7f show that the asynchronous algorithm is sufficiently robust to such communication failures. This aligns with the finding in [40]. The system performance degrades mildly even at 30%-50% communication failure rates. The system fails at an 80% broadcast failure rate with significantly increased generation curtailment, where large ubiquitous delays can occur and impair dual algorithm convergence [56, 57].

5.6. Communication delays

In this section, the impact of systematic communication delays of various time steps is studied. At each time step k, dual information from time step $k - \tau$ is used for the primal update step. Figures 7g and 9a show that the algorithm fails when the ubiquitous delay τ exceeds 2 time steps. This is consistent with the result in [33] but contradicts that in [32]. This difference in results may stem from the different algorithms deployed for OFO where their OFO controller relies only on communication between neighbouring nodes. Our result should, however, raise concerns over the robustness of OFO against those systematic communication delays. The impact of delays can be partially mitigated by choosing more conservative gradient scaling, which is demonstrated in Figs. 7h and 9b. Nevertheless, such delays inevitably introduce oscillations to the system inducing instability and render the algorithm sensitive to the choice of gradient scaling and step sizes. An example is given in Fig. 9c. The algorithm works well when α is increased to 0.5 under no delays but fails if delays are present. Under systematic communication delays, one should consider slowing down the update rate to maintain system stability.

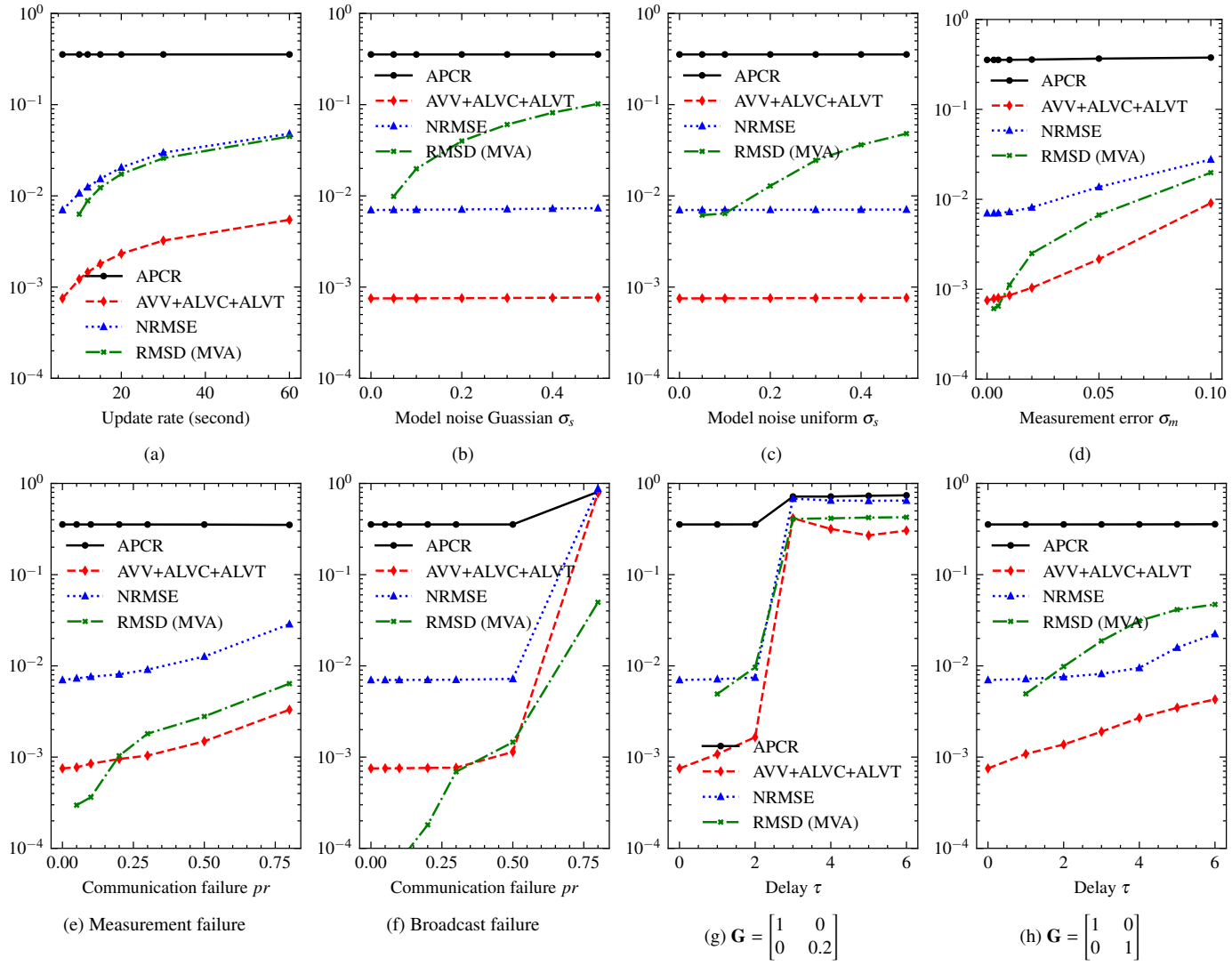

Figure 7: Evaluation metrics under various distribution grid uncertainties. For each uncertain scenario involving grid model inaccuracy, measurement errors, and communication failures, 10 simulations are run with different random seeds and the average results are plotted.

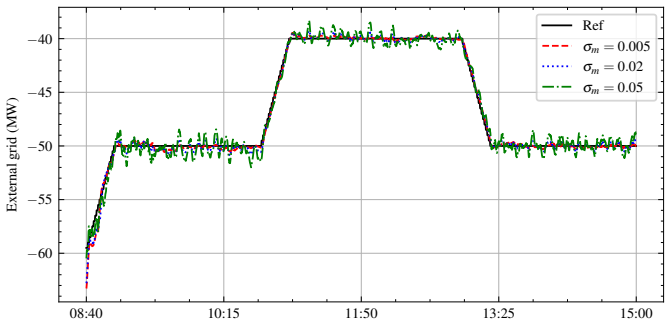

Figure 8: Reference power tracking with measurement errors.

5.7. Topology changes

We consider a scenario where the grid is reconfigured while the DSO is not aware of it. This has not been examined in existing studies as also shown in Table 1. This implies that outdated sensitivity matrices are still in use. We consider cases where one cable trips and the feeder is reconnected by closing one switch ensuring that all loads are restored. In total, 307 cases are built by traversing through all cables and switches and running power flow analyses. The static simulation is run for all 307 cases. We collect AVV, ALVC, ALVT, and NRMSE results for the last 100 iterations and classify the case as *fail* if any of these metrics exceeds 10^{-6} and *success* otherwise. In total 59 cases are classified as *fail*, leading to a failure rate of 19.2%. Figure 10 presents the distribution of successful and failed cases along the tripped cable. It shows that in most failed cases, the tripped cable is located at the beginning section of a distribution feeder. As an example, Fig. 11 shows the loading percentages of two cables at the beginning of the feeder to which the tripped feeder is connected. Overloading issues persist. This is because that PVs located at the tripped feeder have zero sensitivities towards the loading of the connected feeder in the outdated sensitivity matrices. Topology identification, if available, can be a

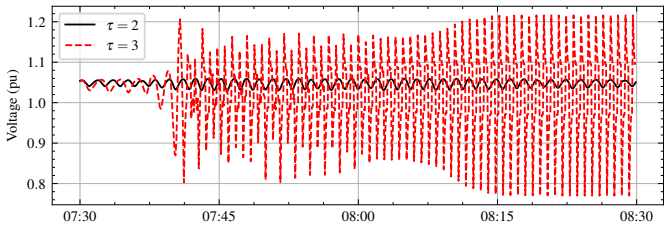

(a) $\mathbf{G} = \begin{bmatrix} 1 & 0 \\ 0 & 0.2 \end{bmatrix}$

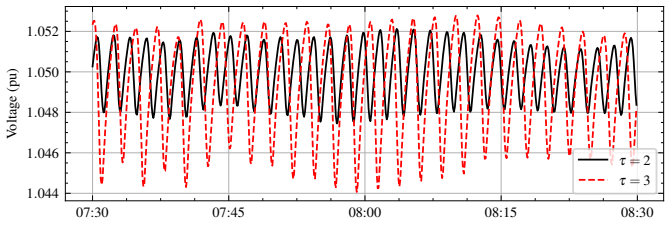

(b) $\mathbf{G} = \begin{bmatrix} 1 & 0 \\ 0 & 1 \end{bmatrix}$

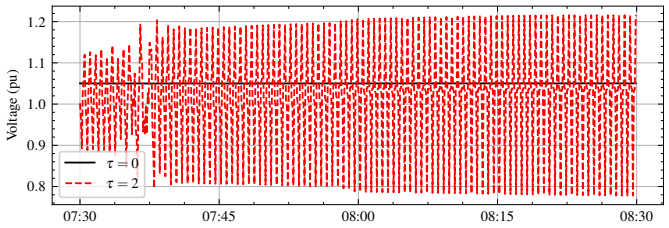

(c) $\mathbf{G} = \begin{bmatrix} 1 & 0 \\ 0 & 1 \end{bmatrix}$, $\alpha = 0.5$

Figure 9: Voltage profiles under various delays, scaling matrices, and step sizes.

potential solution to this. Online sensitivity estimation methods and model-free OFO introduced in Section 1 can also be used at the cost of additional complexity.

5.8. *Multiple uncertainties*

Finally, the interaction of multiple uncertainties is examined. Notably, we do not account for communication delays and topology changes in this simulation as they are already known to significantly compromise system performance. Figure 12 shows the various metrics across 82 cases, including low, medium, and high values for model inaccuracy, measurement errors, missing measurements, and broadcast failures, respectively, alongside the deterministic case (case 0). The observed patterns, such as in constraint violations per 9 cases, are caused by increased communication failure rates. Importantly, the simultaneous presence of multiple uncertainties does not introduce stability issues. In summary, the system demonstrates robustness when confronted with multiple uncertainty sources.

5.9. *Result summary*

Based on the above simulation results, the following insights and recommendations are provided:

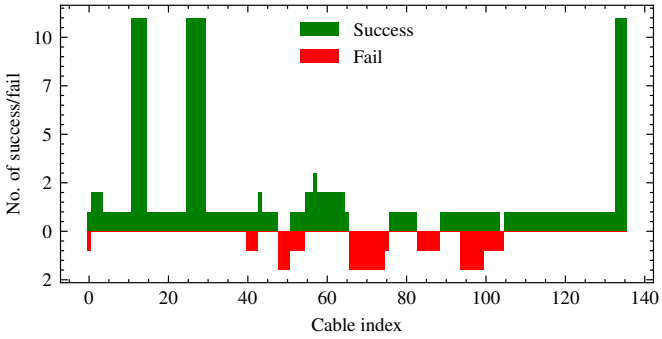

Figure 10: Distribution of successful and failed cases along the tripped cable.

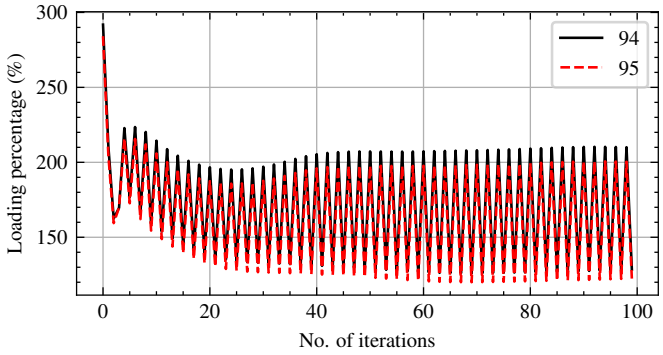

Figure 11: Cable overloading for a network reconfiguration case. Numbered legends represent indices of cables.

- The PDGP-based OFO algorithm demonstrates sufficient robustness to time-varying generation and loads, grid model inaccuracy, measurement errors, communication failures, and their combined presence.
- The algorithm can fail when systematic communication delays exceed some upper bound.
- The algorithm can fail under unobserved topology changes, particularly involving tripping of cables at the beginning of feeders. Topology identification is a potential solution. Online sensitivity estimation and model-free OFO are promising but more complicated.
- Communication delays result in system oscillations and render the algorithm sensitive to the choice of step sizes and gradient scaling.
- Under systematic communication delays, one should consider slowing down the update rate. The update rate should match the communication rate to minimize systematic delays effectively.
- Under severe uncertainties, more conservative gradient scaling and step sizes are recommended. It is advisable to start with small step sizes and $\mathbf{G} = \mathbf{I}$, and then slowly increase step sizes and reduce G_{22} to ensure stability.

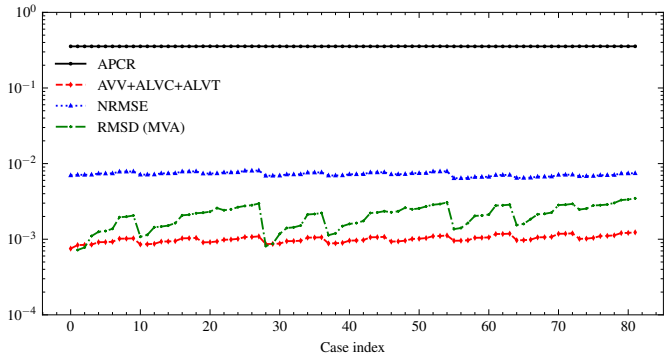

Figure 12: System performance when multiple uncertainties are present. In total 82 cases are examined where $\sigma_s \in \{0.1, 0.2, 0.5\}$, $\sigma_m \in \{0.003, 0.005, 0.01\}$, and $pr \in \{0.05, 0.1, 0.2\}$ for both missing measurements and broadcast failures ($3^4 = 81$), alongside the deterministic case (case 0).

6. Conclusion

In this paper, we numerically assessed the robustness of primal-dual gradient projection-based online feedback optimization. The assessment focused on several distribution grid uncertainties. Active power curtailment, grid constraint violations, and reference power tracking error were evaluated. Simulation results showed that the algorithm demonstrates satisfactory robustness to time-varying generation and loads, grid model inaccuracy, measurement errors, and communication failures, but is more susceptible to systematic communication delays and unobserved topology changes, particularly involving tripping of cables at the beginning of distribution feeders. Potential solutions were proposed to mitigate these uncertainties. This paper will assist distribution system operators in making informed decisions with the deployment of online feedback optimization to manage local grid issues and provide balancing services to transmission system operators. As future work, we are interested in experimentally assessing the algorithm in real-world distribution systems.

Acknowledgement

This work is funded by TKI Urban Enengy from the 'Toeslag voor Topconsortia voor Kennis en Innovatie (TKI)' from the Ministry of Economic Affairs and Climate, under reference 1821401.

References

[1] International Energy Agency, Electricity grids and secure energy transitions, Tech. rep., IEA Publications (2023).

[2] D. K. Molzahn, F. Dörfler, H. Sandberg, S. H. Low, S. Chakrabarti, R. Baldick, J. Lavaei, A survey of distributed optimization and control algorithms for electric power systems, IEEE Trans. Smart Grid 8 (6) (2017) 2941–2962. doi:10.1109/TSG.2017.2720471.

[3] V. Haberle, A. Hauswirth, L. Ortmann, S. Bolognani, F. Dorfler, Non-convex feedback optimization with input and output constraints, IEEE Control Syst. Lett. 5 (1) (2021) 343–348. doi:10.1109/LCSYS.2020.3002152.

[4] A. Hauswirth, Z. He, S. Bolognani, G. Hug, F. Dörfler, Optimization algorithms as robust feedback controllers, Annu. Rev. Control (2024). arXiv:2103.11329.

[5] S. Bolognani, R. Carli, G. Cavraro, S. Zampieri, On the need for communication for voltage regulation of power distribution grids, IEEE Trans. Control Netw. Syst. 6 (3) (2019) 1111–1123. doi:10.1109/TCNS.2019.2921268.

[6] D. Cao, J. Zhao, W. Hu, F. Ding, Q. Huang, Z. Chen, F. Blaabjerg, Data-driven multi-agent deep reinforcement learning for distribution system decentralized voltage control with high penetration of PVs, IEEE Trans. Smart Grid 12 (5) (2021) 4137–4150. doi:10.1109/TSG.2021.3072251.

[7] X. Sun, Y. Tao, J. Zhao, Data-driven combined central and distributed Volt/Var control in active distribution networks, IEEE Trans. Smart Grid (2022) 1–13doi:10.1109/TSG.2022.3213587.

[8] Q. Yang, G. Wang, A. Sadeghi, G. B. Giannakis, J. Sun, Two-timescale voltage control in distribution grids using deep reinforcement learning, IEEE Trans. Smart Grid 11 (3) (2020) 2313–2323. doi:10.1109/TSG.2019.2951769.

[9] Y. Zhang, X. Wang, J. Wang, Y. Zhang, Deep reinforcement learning based Volt-VAR optimization in smart distribution systems, IEEE Trans. Smart Grid 12 (1) (2021) 361–371. doi:10.1109/TSG.2020.3010130.

[10] E. Dall'Anese, A. Simonetto, Optimal power flow pursuit, IEEE Trans. Smart Grid 9 (2) (2018). doi:10.1109/TSG.2016.2571982.

[11] E. Dall'Anese, S. S. Guggilam, A. Simonetto, Y. C. Chen, S. V. Dhople, Optimal regulation of virtual power plants, IEEE Trans. Power Syst. 33 (2) (2018) 1868–1881. doi:10.1109/TPWRS.2017.2741920.

[12] A. Bernstein, E. Dall'Anese, Real-time feedback-based optimization of distribution grids: A unified approach, IEEE Trans. Control Netw. Syst. 6 (3) (2019) 1197–1209. doi:10.1109/TCNS.2019.2929648.

[13] Y. Guo, X. Zhou, C. Zhao, L. Chen, T. H. Summers, Optimal power flow with state estimation in the loop for distribution networks, IEEE Syst. J. 17 (3) (2023) 3694–3705. doi:10.1109/JSYST.2023.3253966.

[14] H. Zhu, H. J. Liu, Fast local voltage control under limited reactive power : Optimality and stability analysis, IEEE Trans. Power Syst. 31 (5) (2016). doi:10.1109/TPWRS.2015.2504419.

[15] A. Hauswirth, A. Zanardi, S. Bolognani, F. Dorfler, G. Hug, Online optimization in closed loop on the power flow manifold, in: 2017 IEEE Manchester PowerTech, Powertech 2017, IEEE, 2017, pp. 1–6. doi:10.1109/PTC.2017.7980998.

[16] M. Picallo, S. Bolognani, F. Dörfler, Closing the loop: Dynamic state estimation and feedback optimization of power grids, Electr. Power Syst. Res. 189 (2020). doi:10.1016/j.epsr.2020.106753.

[17] M. Picallo, L. Ortmann, S. Bolognani, F. Dörfler, Adaptive real-time grid operation via online feedback optimization with sensitivity estimation, Electr. Power Syst. Res. 212 (2022) 108405. doi:10.1016/j.epsr.2022.108405.

[18] R. Cheng, Z. Wang, Y. Guo, An online feedback-based linearized power flow model for unbalanced distribution networks, IEEE Trans. Power Syst. 37 (5) (2022) 3552–3565. arXiv:2103.14820, doi:10.1109/TPWRS.2021.3133257.

[19] T. Xu, W. Wu, Y. Hong, J. Yu, F. Zhang, Data-driven inverter-based volt/var control for partially observable distribution networks, CSEE J. Power Energy Syst. 9 (2) (2023) 548–560. doi:10.17775/CSEEJPES.2020.05920.

[20] M. Colombino, J. W. Simpson-Porco, A. Bernstein, Towards robustness guarantees for feedback-based optimization, in: Proc. IEEE Conf. Decis. Control, IEEE, 2019, pp. 6207–6214. doi:10.1109/CDC40024.2019.9029953.

[21] L. Gan, S. H. Low, An online gradient algorithm for optimal power flow on radial networks, IEEE J. Sel. Areas Commun. (2016). doi:10.1109/JSAC.2016.2525598.

[22] L. Ortmann, J. Maeght, P. Panciatici, F. Dörfler, S. Bolognani, Online feedback optimization for subtransmission grid control, arXiv (2023) 1–9arXiv:2212.07795.

[23] L. Ortmann, G. Hotz, S. Bolognani, F. Dörfler, Real-time curative actions for power systems via online feedback optimization, in: IEEE PowerTech Belgrade, 2023. doi:10.1109/PowerTech55446.2023.10202825.

[24] F. Klein-Helmkamp, F. Böhm, L. Ortmann, A. Winkens, F. Schmidtke, S. Bolognani, F. Dörfler, A. Ulbig, Providing curative distribution grid flexibility using online feedback optimization, in: IEEE PES Innov. Smart Grid Technol. Conf. Eur., 2023. arXiv:2306.14597.

[25] L. Ortmann, S. Bolognani, F. Dörfler, F. Böhm, F. Klein-Helmkamp, A. Ulbig, Tuning and testing an online feedback optimization controller

to provide curative distribution grid flexibility, arXiv (2024). arXiv:2403.01782.

[26] L. Cave, S. Zhan, H. Zhang, N. G. Paterakis, Gradient projection-based online feedback optimization for distribution grid management, in: to appear in CIRED 2024 Work. Vienna, no. June, 2024, pp. 1–5.

[27] S. Bolognani, R. Carli, G. Cavraro, S. Zampieri, Distributed reactive power feedback control for voltage regulation and loss minimization, IEEE Trans. Automat. Contr. 60 (4) (2015). doi:10.1109/TAC.2014.2363931.

[28] L. Ortmann, A. Prostejovsky, K. Heussen, S. Bolognani, Fully distributed peer-to-peer optimal voltage control with minimal model requirements, Electr. Power Syst. Res. 189 (2020) 106717. doi:10.1016/j.epsr.2020.106717.

[29] L. Ortmann, A. Hauswirth, I. Cadu, F. Dörfler, S. Bolognani, Experimental validation of feedback optimization in power distribution grids, Electr. Power Syst. Res. 189 (2020). doi:10.1016/j.epsr.2020.106782.

[30] X. Zhou, E. Dall'anese, L. Chen, Online stochastic optimization of networked distributed energy resources, IEEE Trans. Automat. Contr. 65 (6) (2020) 2387–2401. doi:10.1109/TAC.2019.2927925.

[31] Z. Tang, D. J. Hill, T. Liu, Distributed coordinated reactive power control for voltage regulation in distribution networks, IEEE Trans. Smart Grid 12 (1) (2021). doi:10.1109/TSG.2020.3018633.

[32] S. Magnússon, G. Qu, N. Li, Distributed optimal voltage control with asynchronous and delayed communication, IEEE Trans. Smart Grid 11 (4) (2020). doi:10.1109/TSG.2020.2970768.

[33] N. Patari, A. K. Srivastava, N. Li, Distributed optimal voltage control considering latency and asynchronous communication for three phase unbalanced distribution systems, IEEE Trans. Power Syst. (2022). doi:10.1109/TPWRS.2022.3173634.

[34] X. Zhou, E. Dallanese, L. Chen, A. Simonetto, An incentive-based online optimization framework for distribution grids, IEEE Trans. Automat. Contr. 63 (7) (2018) 2019–2031. doi:10.1109/TAC.2017.2760284.

[35] G. Qu, N. Li, Optimal distributed feedback voltage control under limited reactive power, IEEE Trans. Power Syst. 35 (1) (2020) 315–331. doi:10.1109/TPWRS.2019.2931685.

[36] Y. Chen, A. Bernstein, A. Devraj, S. Meyn, Model-free primal-dual methods for network optimization with application to real-time optimal power flow, in: Proc. Am. Control Conf., no. 5, 2020, pp. 3140–3147. doi:10.23919/ACC45564.2020.9147814.

[37] H. Ipach, L. Fisser, C. Becker, A. Timm-giel, Distributed utility-based real-time power flow optimization in ict-enabled low voltage distribution grids, IET Gener. Transm. Distrib. 17 (13) (2023) 2900–2925. doi:10.1049/gtd2.12653.

[38] T. Zhao, A. Parisio, J. V. Milanović, Distributed control of battery energy storage systems in distribution networks for voltage regulation at transmission-distribution network interconnection points, Control Eng. Pract. 119 (September 2021) (2022) 104988. doi:10.1016/j.conengprac.2021.104988.

[39] C. Hu, X. Zhang, Q. Wu, Gradient-free accelerated event-triggered scheme for constrained network optimization in smart grids, IEEE Trans. Smart Grid PP (8) (2023) 1. doi:10.1109/TSG.2023.3315207.

[40] S. Zhan, J. Morren, W. van den Akker, A. van der Molen, N. G. Paterakis, J. G. Slootweg, Fairness-incorporated online feedback optimization for real-time distribution grid management, IEEE Trans. Smart Grid 15 (2) (2024) 1792–1806. doi:10.1109/TSG.2023.3315481.

[41] M. Panahazari, G. Yao, J. Zhang, Distribution grid services performance analysis for cyber-resilient online feedback-based DER control, in: 2023 IEEE Int. Conf. Commun. Control. Comput. Technol. Smart Grids, IEEE, 2023, pp. 1–6. doi:10.1109/SmartGridComm57358.2023.10333955.

[42] S. Zhan, J. Morren, A. van der Molen, W. van den Akker, N. G. Paterakis, J. G. Slootweg, Multi-timescale coordinated distributed energy resource control combining local and online feedback optimization, Electr. Power Syst. Res. 234 (2024). doi:10.1016/j.epsr.2024.110836.

[43] Y. Tang, K. Dvijotham, S. Low, Real-time optimal power flow, IEEE Trans. Smart Grid 8 (6) (2017). doi:10.1109/TSG.2017.2704922.

[44] R. Cheng, Z. Wang, Y. Guo, Q. Zhang, Online voltage control for unbalanced distribution networks using projected newton method, IEEE Trans. Power Syst. (2022). doi:10.1109/TPWRS.2022.3144246.

[45] S. Zhan, I. Dukovska, W. van den Akker, A. van der Molen, J. Morren, N. G. Paterakis, J. Slootweg, Review of recent developments in technical control approaches for voltage and congestion management in distribution networks, in: IEEE PowerTech, 2023. doi:10.1109/PowerTech55446.2023.10202910.

[46] Z. He, S. Bolognani, J. He, F. Dörfler, X. Guan, Model-free nonlinear feedback optimization, IEEE Trans. Automat. Contr. PP (2022) 1–16. doi:10.1109/TAC.2023.3341752.

[47] H. J. Liu, W. Shi, H. Zhu, Distributed voltage control in distribution networks: Online and robust implementations, IEEE Trans. Smart Grid 9 (6) (2018) 6106–6117. doi:10.1109/TSG.2017.2703642.

[48] M. Alkhraijah, C. Menendez, D. K. Molzahn, Assessing the impacts of nonideal communications on distributed optimal power flow algorithms, Electr. Power Syst. Res. 212 (July) (2022) 108297. doi:10.1016/j.epsr.2022.108297.

[49] S. Paul, N. Gray, A. Dubey, A. Bose, M. Touhiduzzaman, J. Ogle, Robustness assessment of distributed OPF under communication non-idealities using cyber-physical co-simulation framework, in: IEEE IAS Annu. Meet., 2023.

[50] E. Bellini, Grid congestion continues to increase in Netherlands, https://www.pv-magazine.com/2023/01/24/grid-congestion-continues-to-increase-in-netherlands/ (2023).

[51] D. P. Bertsekas, Nonlinear programming, 2nd Edition, Athena Scientific, Massachusetts, 1999. doi:10.1007/BF01582292.

[52] S. Meinecke, D. Sarajlić, S. R. Drauz, A. Klettke, L. P. Lauven, C. Rehtanz, A. Moser, M. Braun, Simbench-a benchmark dataset of electric power systems to compare innovative solutions based on power flow analysis, Energies 13 (12) (2020). doi:10.3390/en13123290.

[53] HelioClim-3 solar radiation database, accessed: Jan. 6, 2023.
URL https://www.soda-pro.com/web-services/radiation/helioclim-3-archives-for-free

[54] Y. Xiang, P. Salemink, B. Stoeller, N. Bharambe, W. van Westering, Power grid model: A high-performance distribution grid calculation library, in: CIRED 2023 - The 27th International Conference and Exhibition on Electricity Distribution, Vol. 2023, 2023, pp. 1–5.

[55] Y. Xiang, P. Salemink, N. Bharambe, M. Govers, J. van den Bogaard, B. Stoeller, Z. Wang, J. Guo, L. Jagutis, C. Wang, M. van Raalte, Contributors to the LF Energy project Power Grid Model, PowerGridModel/power-grid-model. doi:10.5281/zenodo.8054429.
URL https://github.com/PowerGridModel/power-grid-model

[56] S. H. Low, D. E. Lapsley, Optimization flow control - I: Basic algorithm and convergence, IEEE/ACM Trans. Netw. 7 (6) (1999) 861–874. doi:10.1109/90.811451.

[57] Y. Su, Z. Wang, M. Cao, M. Jia, F. Liu, Convergence analysis of dual decomposition algorithm in distributed optimization: Asynchrony and inexactness, IEEE Trans. Automat. Contr. 68 (8) (2023) 4767–4782. doi:10.1109/TAC.2022.3213608.